Giant tunnel electroresistance in two-dimensional ferroelectric tunnel junctions constructed with a Sc_2CO_2/In_2Se_3 van der Waals ferroelectric heterostructure

Aijie Xie,[1,2,3] Hua Hao,[4] Chun-Sheng Liu,[5] Xiaohong Zheng,[3,2,*] Lei Zhang,[6,7,†] and Zhi Zeng[1,2]

[1]*Key Laboratory of Materials Physics, Institute of Solid State Physics, HFIPS, Chinese Academy of Sciences, Hefei 230031, China*
[2]*Science Island Branch of Graduate School, University of Science and Technology of China, Hefei 230026, China*
[3]*College of Information Science and Technology, Nanjing Forestry University, Nanjing 210037, China*
[4]*School of Physics, Hangzhou Normal University, Hangzhou 311121, China*
[5]*College of Electronic and Optical Engineering, Nanjing University of Posts and Telecommunications, Nanjing 210023, China*
[6]*State Key Laboratory of Quantum Optics and Quantum Optics Devices, Institute of Laser Spectroscopy, Shanxi University, Taiyuan 030006, China*
[7]*Collaborative Innovation Center of Extreme Optics, Shanxi University, Taiyuan 030006, China*

(Received 29 December 2022; revised 11 February 2023; accepted 13 March 2023; published 28 March 2023)

Two-dimensional (2D) ferroelectric materials have attracted great attention in recent years due to their thin thickness, high stability, and switchable polarization states. In particular, ferroelectric tunnel junctions (FTJs) constructed from 2D ferroelectric materials have been shown to have very high tunnel electroresistance (TER) ratios. In this work, we design a ferroelectric tunnel junction composed of Sc_2CO_2/In_2Se_3 vertical van der Waals (vdW) heterostructure based on two different 2D ferroelectric materials with out-of-plane polarization. Through density functional calculations combined with a nonequilibrium Green's function technique, it is found that the TER ratio as high as $10^7\%$ can be achieved. Analysis shows that it originates from the difference in the work functions of the contact surfaces of the two ferroelectric materials, which makes charge transfer occur or not occur between them and further leads to a metalinsulator switching of the ferroelectric vdW heterostructure upon the reversion of the applied electrical field. The results suggest the importance of ferroelectric vdW heterostructure in the design of FTJs and a feasible design scheme characterized by proper choice of the work functions and band gaps of the component materials.

DOI: 10.1103/PhysRevB.107.115427

I. INTRODUCTION

Ferroelectric tunnel junctions (FTJs) as a new generation of nonvolatile memory devices have attracted a lot of attention due to the advantages of low energy consumption, high read-write speed, good scalability, and no mechanical damage in operation [1–6]. A typical FTJ consists of a ferroelectric film sandwiched between two metal electrodes, and one of the core problems in the study of FTJs is how to obtain a high tunnel electroresistance (TER) ratio [7,8]. At present, the FTJs that have been studied most frequently are the ones with traditional three-dimensional (3D) ferroelectric materials such as ABO_3-type perovskites as the tunnel barriers [9–12]. However, 3D ferroelectric materials will show two disadvantages in the construction of FTJs when the ferroelectric layer is so thin as below the critical thickness. On one hand, the depolarization field caused by the accumulated polar charge on the surfaces of the film will lead to the disappearance of ferroelectricity. On the other hand, the surface dangling bonds will lead to structural instability. This is in contradiction with the requirement of device miniaturization [13–16]. Therefore, ferroelectric materials that do not suffer from critical thickness that may lead to ferroelectric and structural instabilities are of great interest.

In recent years, together with the rise of two-dimensional (2D) materials, many 2D ferroelectric materials have been proposed theoretically or even prepared experimentally, such as SnTe [17,18], SbN [19], BiP with in-plane spontaneous polarization [20] and In_2Se_3 [21–23], $CuInP_2S_6$ [24,25], Sc_2CO_2 [26], and $AgBiP_2Se_6$ [27]with out-of-plane spontaneous polarization. 2D ferroelectric materials provide a good substitution for the traditional 3D ferroelectric materials in solving the critical thickness problem due to their advantages such as ultrathin atomic thickness, smooth surfaces, and no surface dangling bonds, as well as high structural stability inherent in 2D materials. In fact, 2D FTJs based on 2D ferroelectric materials have been constructed and very high tunnel electroresistance has been reported [28–32]. However, most of the current research focuses on using a single two-dimensional ferroelectric material as the tunnel barrier. It is well known that an emerging direction in the study of 2D materials is the van der Waals (vdW) vertical heterostructure formed by stacking different 2D materials together. vdW heterostructures provide much more freedom for function tuning as compared with single component material. A natural question to ask is, how it will perform when a vdW ferroelectric heterostructure is utilized for constructing 2D FTJs, and further, how shall we design the vdW ferroelectric

*xhzheng@njfu.edu.cn
†zhanglei@sxu.edu.cn

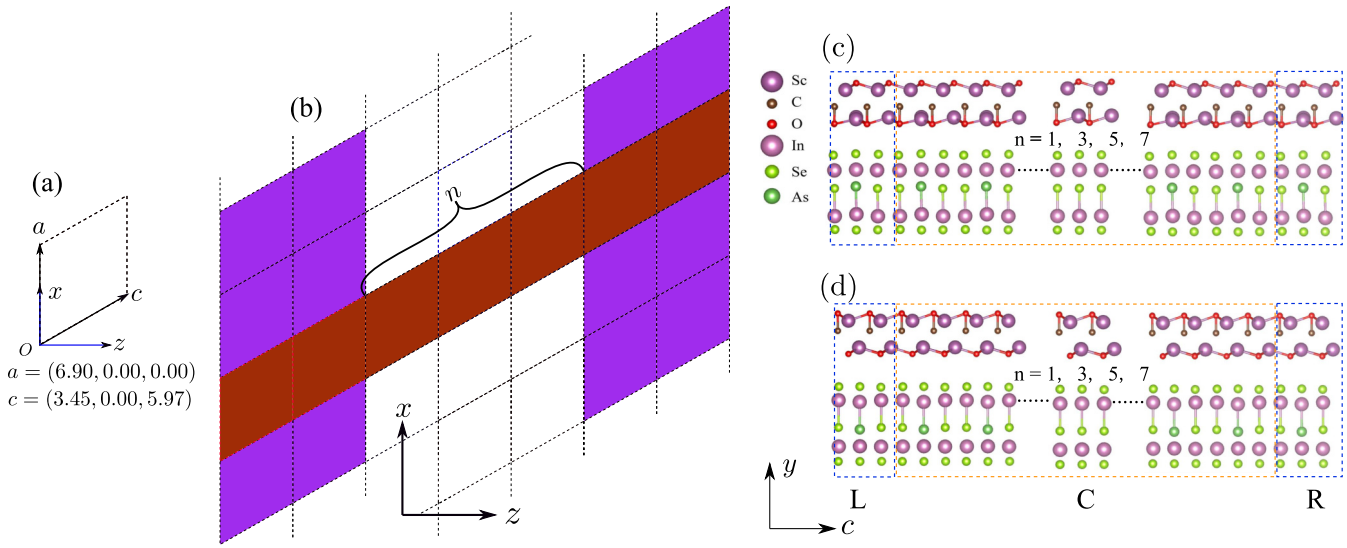

FIG. 1. (a) The electrode supercell with the lattice vectors in the xz plane as $a = (6.90, 0.00, 0.00)$ Å and $c = (3.45, 0.00, 5.97)$ Å. (b) The channel region of the FTJs, with the transport direction along the z direction. The structures of the FTJ with ferroelectric polarizations of both Sc_2CO_2 and In_2Se_3; (c) pointing downward ($P_{\downarrow\downarrow}$) and (d) pointing upward ($P_{\uparrow\uparrow}$), with the blue dashed line region representing the electrode supercell and the red dashed line region representing the channel region. n is the number of pristine Sc_2CO_2/In_2Se_3 supercells included in the channel region.

heterostructure so that FTJs constructed with it will show an excellent giant tunnel electroresistance?

In this work, we intend to construct 2D FTJs with vdW ferroelectric heterostructure materials to realize a giant tunnel electroresistance. In our previous works, we have found that a 2D ferroelectric material can be switched between an insulating state and a metallic state when it is in contact with a metal if the work function of one surface of the ferroelectric materials is nearly equal to that of the metal [28,29]. Generally, the two surfaces of a ferroelectric material with out-of-plane polarization have different work functions with a large difference due to the internal polarization field. When the metal contacted with it has a work function very close to one of its work functions, charge transfer will not occur so that the ferroelectric materials will still be in the insulating state. However, if the polarization of the ferroelectric material is reversed by a vertical electric field, the contacted surface of the ferroelectric material and the metal will have a big difference in the work functions, such that charge transfer will occur between them and the ferroelectric material will change from an insulator to a metal. In this work, although the two 2D ferroelectric materials are both insulators themselves, when the two contacted surfaces between the two materials have close and much different work functions, charge transfer is expected to occur or not occur between them, and the vdW heterostructure will have two different states: namely, an insulating state and a metallic state. This will serve as the physical basis for the design of FTJs with a large tunnel electroresistance using 2D vdW ferroelectric materials.

To implement this idea, we select two different 2D ferroelectric materials Sc_2CO_2 and In_2Se_3 with out-of-plane polarization to form a vdW heterostructure and take it as the tunnel barrier to construct a FTJ. To obtain metallic leads, we take a scheme by doping the same material, as seen frequently in literature [31,32]. Namely, all the left lead, central region, and the right lead are served by the same material, but with the leads doped and the central region not. To be specific, the doping in our work is realized by substituting part of the internal Se atoms in In_2Se_3. Based on density functional calculations, we find that Sc_2CO_2 and In_2Se_3 remain in the insulator state when the polarization in both ferroelectric materials point upward, while an insulator-to-metal transition occurs in both In_2Se_3 and Sc_2CO_2 materials when the polarizations in both materials are reversed simultaneously to point down due to the appropriate work function difference between them. As a result from this, the designed FTJ may exhibit a giant TER ratio up to 10^7%.

II. STRUCTURE AND COMPUTATION DETAILS

The Sc_2CO_2 rhombic cell size is 3.42 Å × 3.42 Å and the In_2Se_3 rhombic cell size is 4.11 Å × 4.11 Å in the xz plane. For the electrode supercell, we choose 2×2 Sc_2CO_2 unit cells and $\sqrt{3} \times \sqrt{3}$ In_2Se_3 unit cells. In this way, the lattice mismatch of the two ferroelectric materials is less than 4%. After full relaxation, we get the lattice constant of the electrode supercell in the xz plane as 6.90×6.90, with the lattice vectors $a = (6.90, 0.00, 0.00)$ Å, $b = (0.00, 45.00, 0.00)$ Å, and $c = (3.45, 0.00, 5.97)$ Å [see Fig. 1(a)]. The device is constructed by periodically repeating this supercell along the a and c directions before doping the electrodes [see Fig. 1(b)]. The red region in Fig. 1(b) shows one device cell, and the device is periodic along the a direction. For the channel region, we consider two electrode supercells on each side along the c direction as the buffer layers together with $n = 1$, 3, 5, and 7 Sc_2CO_2/In_2Se_3 supercells, respectively. The vacuum thickness of more than 30 Å in the y direction is adopted to avoid the interaction between adjacent repeating cells. Thus, the system is periodic along the x direction and the transport direction is along the z axis. Figures 1(c) and 1(d) show the

structures of the Sc_2CO_2/In_2Se_3 based FTJ, with Sc_2CO_2 and In_2Se_3 both polarized downward ($P_{\downarrow\downarrow}$) and both polarized upward ($P_{\uparrow\uparrow}$), respectively. The jucntion is divided into three parts: left (L) and right (R) leads, and central scattering region (C). The left/right leads are $Sc_2CO_2/In_2Se_3(As_{Se-i})$ vdW vertical heterostructures, where $In_2Se_3(As_{Se-i})$ means one of the internal Se atoms in each electrode supercell is substituted by an As atom, and i stands for "internal". The central region (channel) is Sc_2CO_2/In_2Se_3 vdW vertical heterostructure.

The structural relaxations and electronic structure calculations are performed by density functional theory (DFT) as implemented in the Vienna *ab initio* simulation package (VASP) [33–35]. The generalized gradient approximation (GGA) with a form of Perdew-Burke-Ernzerhof (PBE) is adopted for the exchange-correlation potential [36], and the energy cutoff is set to 500 eV. vdW interaction is considered in the atomic relaxation using the DFT-D3 method, and the k-point sampling grid is chosen as $6 \times 1 \times 6$. All structures are optimized until the Hellmann-Feynman force is below 0.01 eV/Å and the convergence threshold of the electron energy is 10^{-6} eV. To avoid the effect of the vacuum electric field, a dipole correction is applied [37].

The quantum transport calculations are performed using the Nanodcal package [38] based on the DFT and nonequilibrium Green's function (NEGF) technique [39]. The exchange-correlation functional takes the same PBE form of GGA as above. The k-point grid in the self-consistent calculation is set to $4 \times 1 \times 1$, whereas it is chosen as $100 \times 1 \times 1$ in the calculation of the transmission function since it demands a much denser k grid. The tunneling equilibrium conductance of the system is obtained from the following equation:

$$G = \frac{2e^2}{h} \sum_{k_x} T(k_x, E), \tag{1}$$

where $T(k_x, E)$ is the transmission function of the electronic state at $k = k_x$ for energy E. Further, the TER ratio of the system is calculated by [10]

$$TER = \frac{|G_\uparrow - G_\downarrow|}{\min(G_\uparrow, G_\downarrow)}, \tag{2}$$

where $G_\uparrow$ and $G_\downarrow$ are the tunneling equilibrium conductances of the ferroelectric tunnel junction when the ferroelectric layer is in the polarization up ($P_\uparrow$) and polarization down ($P_\downarrow$) states, respectively.

III. RESULTS AND DISCUSSION

First, we study the geometric structure and electronic properties of the proposed 2D ferroelectric Sc_2CO_2/In_2Se_3 vdW heterostructure. Both component materials Sc_2CO_2 and In_2Se_3 have large out-of-plane polarization due to the displacement of the intermediate C and Se atoms, respectively. From our calculations, a band gap of 1.80 eV and polarization intensity of 0.098 eÅ/unit cell is obtained for Sc_2CO_2, and a band gap of 0.76 eV and polarization intensity of 0.095 eÅ/unit cell is obtained for In_2Se_3, which is consistent with previous reports [23,26]. The Sc_2CO_2/In_2Se_3 vdW vertical heterostructure is then formed by stacking Sc_2CO_2 above In_2Se_3. In the structural relaxation, we consider three

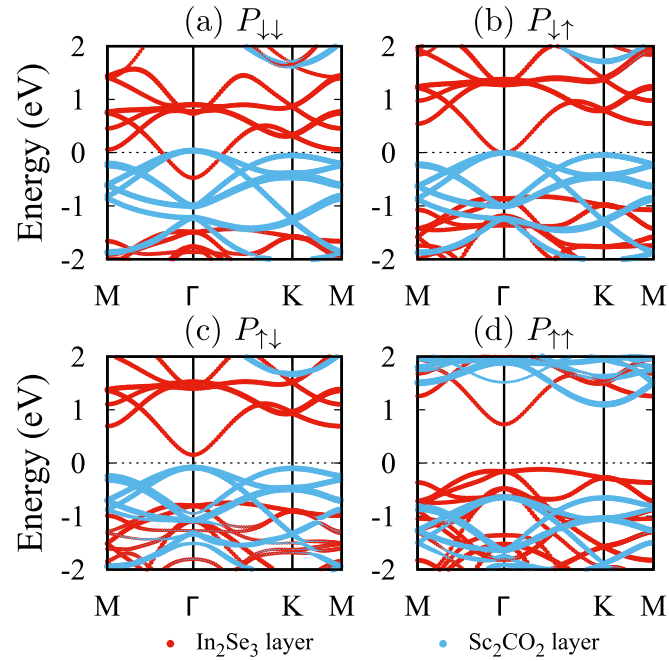

FIG. 2. The layer-resolved band structure for the state: (a) $P_{\downarrow\downarrow}$, (b) $P_{\downarrow\uparrow}$, (c) $P_{\uparrow\downarrow}$,; and (d) $P_{\uparrow\uparrow}$. The Fermi level is set to 0 eV.

configurations of Sc_2CO_2/In_2Se_3 heterostructure with high symmetry; namely, configuration 1 in which the C and O atoms of the Sc_2CO_2 layer are located right above the top Se atom of the In_2Se_3 layer, configuration 2 in which the Sc atoms of the Sc_2CO_2 layer are located above the top Se atoms of the In_2Se_3 layer, and configuration 3 in which the Sc and O atoms of the Sc_2CO_2 layer are located above the top Se atoms of the In_2Se_3 layer. Eventually, we find that the difference in energy between the three configurations is negligibly small, less than 1 meV, and the difference in the band structures of them is also negligibly small. We will select the fully optimized configuration 1 with an optimized lattice constant of 6.90 Å for our further construction of FTJ.

There are four possible different polarization states for vdW heterostructure, namely, $P_{\downarrow\downarrow}$, $P_{\downarrow\uparrow}$, $P_{\uparrow\downarrow}$, and $P_{\uparrow\uparrow}$, where the first and second arrows indicate the polarization directions of the Sc_2CO_2 and In_2Se_3 layers, respectively. The fully relaxed interlayer distance is 2.93, 2.98, 3.03, and 3.07 Å, respectively, and the geometrical parameters of Sc_2CO_2 and In_2Se_3 layers change negligibly with the reversion of the ferroelectric polarization. The layer-resolved band structures of these four polarization cases are shown in Fig. 2. Very interestingly, the $P_{\downarrow\downarrow}$ and $P_{\downarrow\uparrow}$ states become metallic. In the $P_{\downarrow\downarrow}$ case, the overlap between the valence band of Sc_2CO_2 and the conduction band of In_2Se_3 is very large while in the $P_{\downarrow\uparrow}$, the valence band maximum and the conduction band minimum just touch at the Fermi level. In contrast, the $P_{\uparrow\downarrow}$ and $P_{\uparrow\uparrow}$ cases are both insulators, with the band gap of $P_{\uparrow\downarrow}$ much smaller than that of $P_{\uparrow\uparrow}$. In the following, the FTJs in only the $P_{\downarrow\downarrow}$ and $P_{\uparrow\uparrow}$ states will be considered for two reasons. On one hand, the uniformly polarized states, namely $P_{\downarrow\downarrow}$ and $P_{\uparrow\uparrow}$, are the easiest to obtain since they can always be achieved by applying strong enough electric field with opposite directions. On the other hand, the difference in the conductivity between

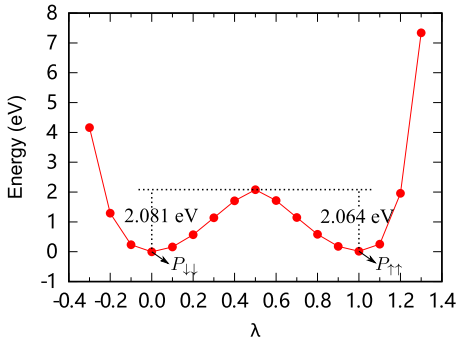

FIG. 3. The switching pathway between $P_{\downarrow\downarrow}$ and $P_{\uparrow\uparrow}$. $\lambda = 0.0$ and $\lambda = 1.0$ represent the $P_{\downarrow\downarrow}$ and $P_{\uparrow\uparrow}$ states, respectively. The energy of $P_{\downarrow\downarrow}$ is set to 0 eV.

these two states are the biggest since $P_{\downarrow\downarrow}$ is a good metal with bands from both the Sc_2CO_2 and In_2Se_3 layers crossing the Fermi level, while $P_{\uparrow\uparrow}$ is an insulator with a large band gap. In addition, the total energy of $P_{\downarrow\downarrow}$ is 0.17 eV lower than that of $P_{\uparrow\uparrow}$. The bistable nature is confirmed by calculating the switching pathway and barrier between these two opposite polarization states, which is realized by carrying out a series of static calculations along the pathway generated through a linear interpolation of the atomic coordinates, namely $\vec{r} = (1-\lambda)\,\vec{r}\,(P_{\downarrow\downarrow}) + \lambda\,\vec{r}\,(P_{\uparrow\uparrow})$. The switching pathway is shown in Fig. 3. It clearly shows that the two states are stable, with a barrier height of 2.081 eV from $P_{\downarrow\downarrow}$ to $P_{\uparrow\uparrow}$, and 2.064 eV from $P_{\uparrow\uparrow}$ to $P_{\downarrow\downarrow}$.

The electrode is achieved by doping As in the Sc_2CO_2/In_2Se_3 vdW heterostructure, and in detail by replacing one internal Se atom of the In_2Se_3 layer. Since As($4s^24p^2$) has one less valence electron than Se($4s^24p^3$), $In_2Se_3(As_{Se-i})$ can be considered as p type doped, where the Fermi energy (E_F) is shifted below the top of the valence band by hole doping, as shown in Fig. 4(a). We calculated the formation energy of As doping, which is defined as $E_{\text{form}} = E(In_xSe_yAs_z) - xE(\text{In}) - yE(\text{Se}) - zE(\text{As})$. We get $E_{\text{form}} = -0.1618$ eV/Å^2, suggesting the feasibility of As doping in In_2Se_3, which is consistent with literature [40]. Further, As-doped In_2Se_3 is magnetic and halfmetallic, as indicated by the band structure shown in Fig. 4(a). When the $In_2Se_3(As_{Se-i})$ is stacked with Sc_2CO_2, the vdW heterostructure is still conducting, with the bands crossing the Fermi level coming from the valence bands of Sc_2CO_2 in the $P_{\downarrow\downarrow}$ state [see Fig. 4(b)],

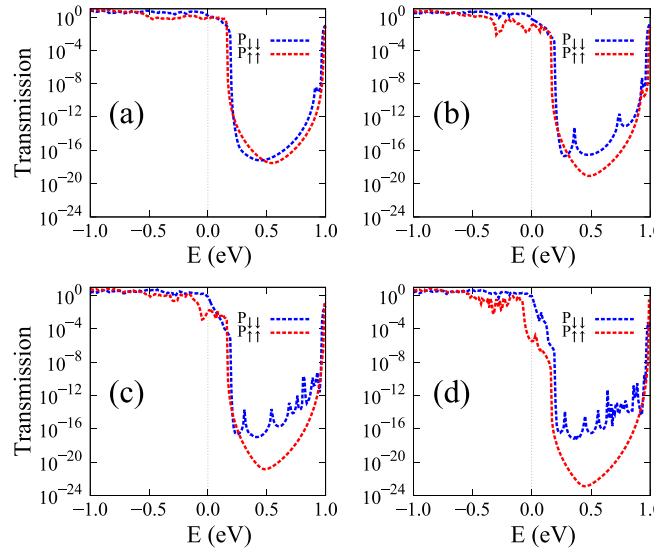

FIG. 5. The transmission functions of the $P_{\downarrow\downarrow}$ and $P_{\uparrow\uparrow}$ states when the transport channel length. (a) $n = 1$, (b) $n = 3$, (c) $n = 5$, and (d) $n = 7$. The Fermi level is set to 0 eV.

but with bands crossing the Fermi level coming from the spin down channel of the valence bands of $In_2Se_3(As_{Se-i})$ in the $P_{\uparrow\uparrow}$ state [see Fig. 4(c)]. Next, we calculate the transmission functions of the FTJ in the $P_{\downarrow\downarrow}$ and $P_{\uparrow\uparrow}$ states in the following. In addition, we have considered the length effect by choosing $n = 1$, 3, 5, and 7 supercells of the undoped Sc_2CO_2/In_2Se_3 heterostructure in the tunnel barrier. As shown in Fig. 5, it is found that the transmission (summed over the two spin channels) near the Fermi level in the case of $P_{\downarrow\downarrow}$ is always larger than that in the case of $P_{\uparrow\uparrow}$. With the increase of the channel length n, the transmission at the Fermi level in the case of $P_{\downarrow\downarrow}$ changes very little, while the transmission in the case of $P_{\uparrow\uparrow}$ drops substantially. The TER ratios of the FTJs defined by the tunnel equilibrium conductance are calculated to be 72.2%, 397.6%, 6126.9%, and 2.6×10^7%, respectively, when $n = 1, 3, 5$, and 7, increasing nearly exponentially, as shown in Fig. 6(a). For the case of $n = 7$, the TER ratio as a function of energy is shown in Fig. 6(b) and it is larger than 10^6% in a large energy range around the Fermi level, which is larger than the previously reported TER ratio of FTJs composed of a single 2D ferroelectric material [41,42].

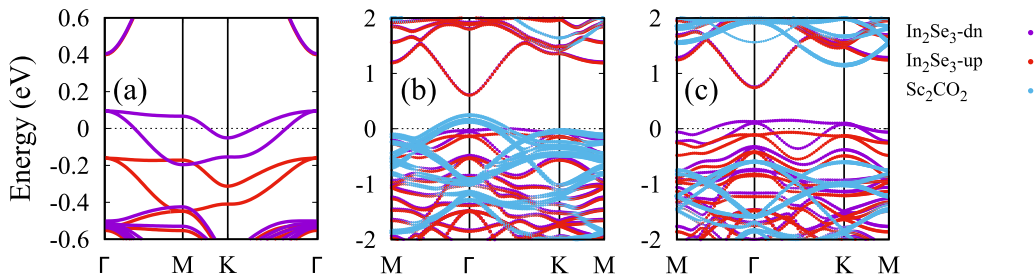

FIG. 4. The band structure of (a) $In_2Se_3(As_{Se-i})$, (b) the $P_{\downarrow\downarrow}$ state of $Sc_2CO_2/In_2Se_3(As_{Se-i})$, and (c) the $P_{\uparrow\uparrow}$ state of $Sc_2CO_2/In_2Se_3(As_{Se-i})$.

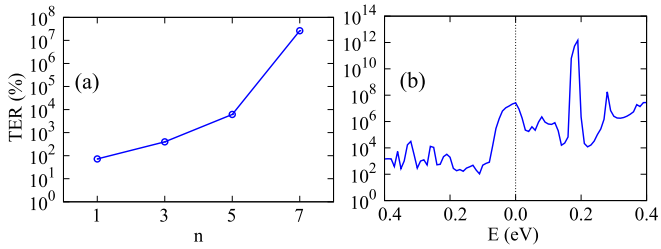

FIG. 6. (a) The TER ratio at the Fermi level as a function of the channel length n. (b) The TER ratio as a function of electron energy at $n = 7$.

To study the origin of the giant TER ratio, we analyze the layer-resolved projected density of states (summed over the two spin channels) of the central region in the $P_{\downarrow\downarrow}$ and $P_{\uparrow\uparrow}$ polarization cases for the length $n = 7$, as shown in Fig. 7. Here, one "layer" means one "supercell" along the z direction. In the $P_{\downarrow\downarrow}$ case, each layer is metallic and no gap is found around the Fermi level. In contrast, in the $P_{\uparrow\uparrow}$ case, there is a large band gap above the Fermi level and the Fermi level just cuts the tail of the valence band of In_2Se_3. This obviously originates from the intrinsic nature of the pristine Sc_2CO_2/In_2Se_3 heterostructure which is metallic in the $P_{\downarrow\downarrow}$ case and insulating in the $P_{\uparrow\uparrow}$ case. Thus, it is important to understand why the $P_{\downarrow\downarrow}$ is metallized while the $P_{\uparrow\uparrow}$ is insulative. Clearly, from the band structure in the $P_{\downarrow\downarrow}$ state as shown in Fig. 2(a), there is charge transfer from Sc_2CO_2 to In_2Se_3 since both the valence band of Sc_2CO_2 and the conduction band of In_2Se_3 become partially filled due to charge redistribution between them. In contrast, in the $P_{\uparrow\uparrow}$ case, no charge transfer occurs.

For two insulators stacked together, charge transfer will occur only when the conduction band minimum (CBM) of one material (M1) gets below the valence band maximum (VBM) of the other material (M2) due to the relative shift of the energy bands of the two materials. The driving force for this relative band shift is the contact potential, which actually originates from the difference in the Fermi levels (VBMs for pristine semiconductors or insulators) of the two contacted materials, or equivalently, the work functions since the work function is simply defined as the difference between the vacuum level and the Fermi level, namely,

$$W = E_{\text{vac}} - E_F, \tag{3}$$

and the vacuum levels E_{vac} of two different materials will be aligned equal when stacked together. The vacuum level of a surface is obtained by the saturated constant value of the electrostatic potential along the vertical direction when it goes away from it [see Fig. 8(b)]. For a 2D material with out of plane polarization, due to the internal polarization field, the vacuum levels of the two surfaces are different, while the Fermi energy is the same. Thus, it will have two different vacuum levels on the opposite sides [see Fig. 8(b)], which produce two different work functions. Suppose the two materials have work functions W_1 and W_2 (with $W_1 > W_2$), and Fermi levels E_{F1} and E_{F2} (with $E_{F1} < E_{F2}$), as shown in Fig. 8(a). When two different materials are stacked together, due to the different work functions, the Fermi level positions must be different, and the difference (ΔE_F) in the Fermi levels will produce the contact potential difference which leads to the existence of a built-in electric field $\vec{E}$ directing from left to right across the interface. This built-in electric field will produce a potential gradient directing from right to left for electrons, which will lead to the movement of the energy bands of them toward opposite directions [43]. In the case of Fig. 8(a), the bands shift down in M1 and up in M2. From this analysis, we conclude that the energy level will shift down at the larger work function side and shift up at the lower work function side. The possible maximum shift is ΔE_F since finally the Fermi levels of the two materials will become equal and the heterostructure will establish a common Fermi level. When the CBM of M1 gets below theVBM of M2, charge transfer starts to occur between them. For M1, it means that the Fermi level should shift from the VBM to the CBM, which is the band gap E_{g1} of M1. Thus, in order for the charge transfer to occur, we should have at least $E_{g1} < \Delta W (= \Delta E_F)$, namely, the band gap at the larger work function side should be smaller than the ΔW. Note that when applying the equation $E_{g1} < \Delta W$, E_{g1} is always defined as the band gap of the material

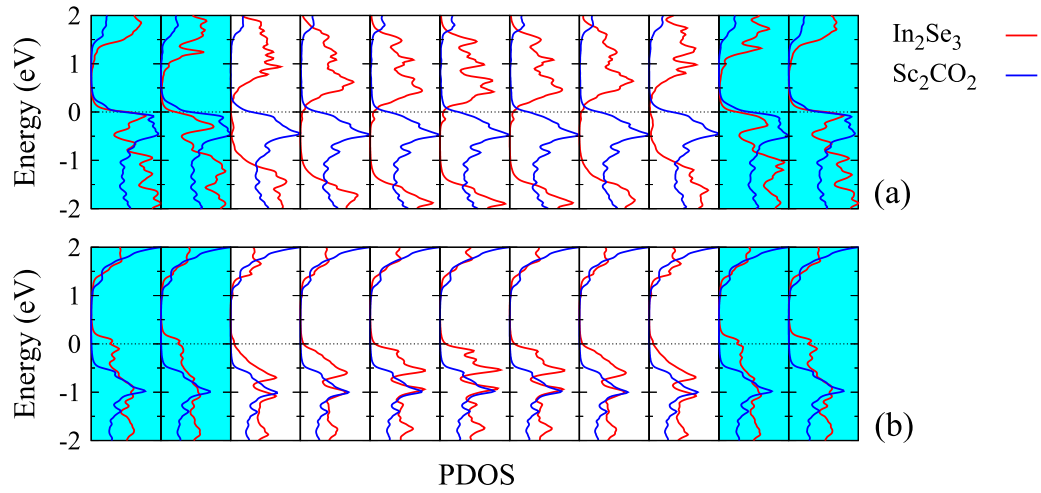

FIG. 7. The layer-resolved projected density of states (PDOS) of the central region of the FTJ for (a) the $P_{\downarrow\downarrow}$ state, (b) the $P_{\uparrow\uparrow}$ state.

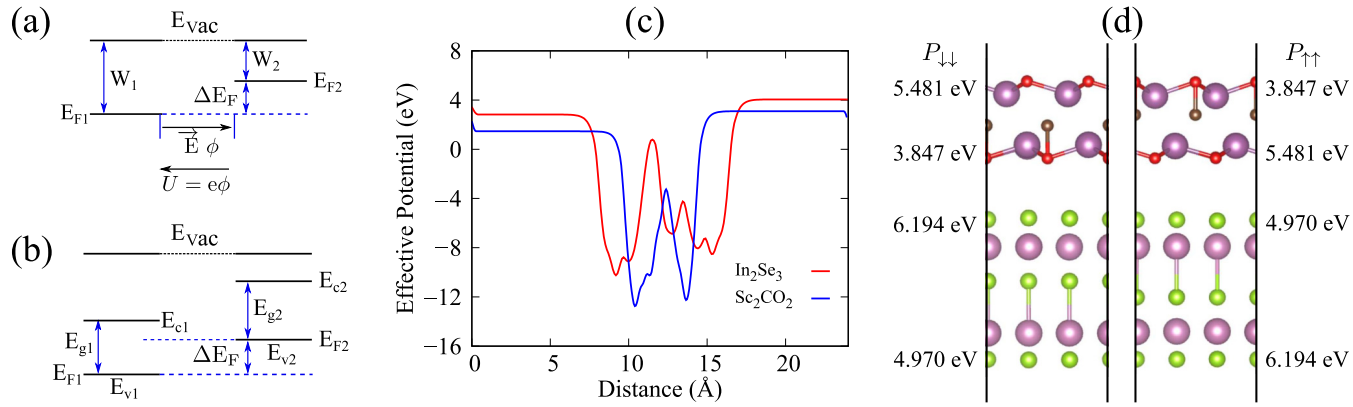

FIG. 8. (a) The schematic model for the formation of the contact potential between two different materials; (b) the band alignment of two different semiconductors in contact before a common Fermi level is established; (c) the effective potentials of Sc_2CO_2 (blue solid line), and In_2Se_3 (red solid line) along the vertical direction of the vacuum layer (in the figure, the out-of-plane polarization in each separate material points from right to left); and (d) the work functions of Sc_2CO_2, and In_2Se_3 in the $P_{\downarrow\downarrow}$ state (left panel) and the $P_{\uparrow\uparrow}$ state (right panel).

whose surface in contact has a larger work function than that of the other material.

Based on the arguments above, we can understand the four different band structures in Fig. 2 when the two ferroelectric materials are stacked together. The band gaps are calculated to be 1.80 eV for Sc_2CO_2 and 0.76 eV for In_2Se_3. Each 2D ferroelectric material with out of plane polarization has different vacuum levels at the two surfaces due to the broken symmetry in the vertical direction [see Fig. 8(c)], which means that it will have two different work functions. As shown in Fig. 8(d), we calculate the work functions for Sc_2CO_2 as 5.841 eV (negatively charged side) and 3.847 eV (positively charged side), and for In_2Se_3 as 6.194 eV (negatively charged side) and 4.970 eV (positively charged side), respectively. In the $P_{\downarrow\downarrow}$ state, the work functions of the contacted surfaces will be 3.847 eV for Sc_2CO_2 and 6.194 eV for In_2Se_3 [see left panel in Fig. 8(d)], which results in $\Delta W = 2.347$ eV. Thus, the energy bands of In_2Se_3 will shift down relative to Sc_2CO_2. Further, since the band gap of the larger work function side of In_2Se_3 ($E_{g1} = 0.76$ eV) is much smaller than $\Delta W = 2.347$ eV, the CBM of In_2Se_3 can shift far below the VBM of Sc_2CO_2. Thus, charge transfer occurs and both materials become metallic. In the $P_{\uparrow\uparrow}$ state, the work functions of the contacted surfaces will be 5.481 eV for Sc_2CO_2 and 4.970 eV for In_2Se_3 [see right panel in Fig. 8(d)], which results in $\Delta W = 0.511$ eV. In this case, the energy bands of Sc_2CO_2 will shift down relative to those of In_2Se_3 since the work function of the contacted surface of Sc_2CO_2 is larger. In this case, E_{g1} is the band gap of Sc_2CO_2, namely $E_{g1} =$ 1.80 eV, which is larger than $\Delta W = 0.511$ eV. Thus, although the bands of Sc_2CO_2 shift down, its CBM can not get below the VBM of In_2Se_3. Consequently, no charge transfer occurs and both materials are still insulators. With similar analysis, we can understand the band structures of $P_{\downarrow\uparrow}$ and $P_{\uparrow\downarrow}$ shown in Figs. 2(b) and 2(c). For the $P_{\downarrow\uparrow}$ case, the contacted surface of the In_2Se_3 has a larger work function (4.970 eV) than that (3.847 eV) of Sc_2CO_2. Thus, the band gap of In_2Se_3 is defined as E_{g1}. For this case, the work function difference is $\Delta W =$ $4.970 - 3.847 = 1.123 > E_{g1} = 0.76$ eV. Thus, the relation $E_{g1} < \Delta W$ holds and the two materials will become metallic [compare with Fig. 2(b)]. For the $P_{\uparrow\downarrow}$ case, the contacted surface of the In_2Se_3 has a larger work function (6.194 eV) than that (5.481 eV) of Sc_2CO_2. Thus the band gap of In_2Se_3 is defined as E_{g1}. For this case, the work function difference is $\Delta W = 6.194 - 5.481 = 0.713$ eV $< E_{g1} = 0.76$ eV. Therefore, the relation $E_{g1} < \Delta W$ does not hold and the two materials will not become metallic [compare with Fig. 2(c)]. Therefore, the relation $E_{g1} < \Delta W$ predicts the band structures shown in Fig. 2 very well. Of course, it is well known that the band gap is systematically underestimated by the GGA-PBE functional. Since the giant tunnel electroresistance of the FTJ depends on the metallic and insulating characters in the two polarization states, it is important that the transition from metal to insulator should still happen when the polarization changes from $P_{\downarrow\downarrow}$ to $P_{\uparrow\uparrow}$ in more accurate calculations with an advanced Heyd-Scuseria-Ernzerhof (HSE) functional [44]. We have specifically checked the band structures for the $P_{\downarrow\downarrow}$ to $P_{\uparrow\uparrow}$ cases, based on which we build the FTJs. Seen from the band structures in Figs. 9(a) and 9(b), we find that the conclusion is the same; namely, $P_{\downarrow\downarrow}$ is metallic and $P_{\uparrow\uparrow}$ is insulating. The main difference is that in the insulating $P_{\uparrow\uparrow}$ case, the conduction bands are pushed to a much higher position. It also agrees well with the mechanism explanation based on the equation $E_{g1} < \Delta W$ as given above. With HSE, we got the band gap as 1.43 eV for In_2Se_3 and 2.89 eV for Sc_2CO_2, in good agreement with the literature [23,26]. The work functions are marked in Fig. 9(c). We find that $E_{g1}(In_2Se_3)$ $= 1.43$ eV and $\Delta W = 2.667$ eV in the $P_{\downarrow\downarrow}$ state, thus the two materials will become metallic according to the condition $E_{g1} < \Delta W$. In contrast, in the $P_{\uparrow\uparrow}$ state, $E_{g1}(Sc_2CO_2)$ $= 2.89$ eV and $\Delta W = 0.592$ eV; we will have $E_{g1} > \Delta W$, thus the two materials will be insulating.

Finally, we briefly explain the length dependence of the TER ratio. When $n = 1$, due to the electrode effects, both the $P_{\downarrow\downarrow}$ and the $P_{\uparrow\uparrow}$ states are metal-like, thus the difference between the two states is small and the TER ratio is also small. With the increase of channel length, the electrode effect decreases and the insulating nature of the $P_{\uparrow\uparrow}$ state in the channel starts to become more and more clear, thus the difference in the equilibrium conductance between the two states increases

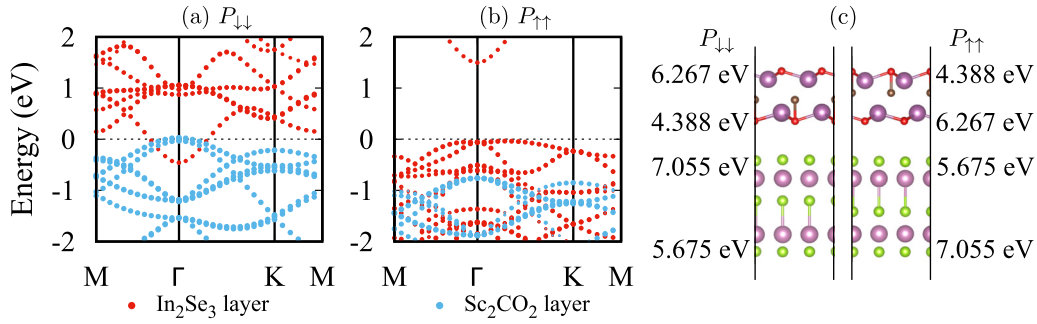

FIG. 9. The band structures with HSE functional for (a) the $P_{\downarrow\downarrow}$ state and (b) the $P_{\uparrow\uparrow}$ state. (c) The work functions of Sc_2CO_2 and In_2Se_3 in the $P_{\downarrow\downarrow}$ state (left panel) and the $P_{\uparrow\uparrow}$ state (right panel).

rapidly. For $n = 7$, we can already get the TER ratio as large as $10^7\%$, and it is expected to be even larger with further increase in n.

IV. CONCLUSION

In summary, we have designed a 2D FTJ composed of vertical vdW heterostructures using two different 2D ferroelectric materials (Sc_2CO_2 and In_2Se_3) with out-of-plane polarization, and investigated the electronic structure of the Sc_2CO_2/In_2Se_3 heterostructure and the electrical behavior of the FTJ using $Sc_2CO_2/In_2Se_3(As_{Se-i})$ as the electrode and Sc_2CO_2/In_2Se_3 as the transport channel. We found that in the case of $P_{\downarrow\downarrow}$, both the Sc_2CO_2 and In_2Se_3 layers are transformed into a metallic state, while in the case of $P_{\uparrow\uparrow}$, they both remain in an insulating state. Further analysis of the electronic structure shows that in $P_{\downarrow\downarrow}$, a large difference (about 2.347 eV) in the work functions of the two contacted surfaces and the small band gap of In_2Se_3 layers cause the CBM of In_2Se_3 to be below the VBM of Sc_2CO_2 which leads to the transfer of electrons from Sc_2CO_2 to In_2Se_3. In the $P_{\uparrow\uparrow}$ state, the small difference (0.511 eV) in the work functions of the two contacted surfaces and the big band gap (1.80 eV) of function of the Sc_2CO_2 cannot cause the CBM of Sc_2CO_2 to be below the VBM of In_2Se_3; thus, there is no charge transfer and both materials are still insulators. These two states lead to greatly different tunneling equilibrium conductances in the different polarization states and eventually reach a giant TER ratio of $10^7\%$ when the channel length satisfies $n \geqslant 7$. These studies suggest the importance of 2D vdW ferroelectric materials in the design of FTJs, and a feasible design principle of high performance FTJs with 2D bilayer vdW ferroelectric materials based on the work function difference and band gap of the two component ferroelectric materials.

ACKNOWLEDGMENTS

We gratefully acknowledge the support from the National Natural Science Foundation of China (Grants No. 11974355, No. 61974068, and No. 12074230); National Key R&D Program of China (Grant No. 2022YFA1404003); Shanxi Province 100-Plan Talent Program and the Fund for Shanxi "1331 Project." A.X. was partially supported by the postgraduate research opportunities program of HZWTECH (HZWTECH-PROP). Calculations were performed in the Center for Computational Science of CASHIPS, the ScGrid of Supercomputing Center, and Computer Network Information Center of Chinese Academy of Sciences.

[1] S. Yuan, J. Wang, X. Zhong, F. Wang, B. Li, and Y. Zhou, A ferroelectric tunnel junction based on the piezoelectric effect for non-volatile nanoferroelectric devices, J. Mater. Chem. C **1**, 418 (2013).

[2] M. Dawber, K. M. Rabe, and J. F. Scott, Physics of thin-film ferroelectric oxides, Rev. Mod. Phys. **77**, 1083 (2005).

[3] J. F. Scott, Applications of modern ferroelectrics, Science **315**, 954 (2007).

[4] D. J. Kim, H. Lu, S. Ryu, C.-W. Bark, C.-B. Eom, E. Y. Tsymbal, and A. Gruverman, Ferroelectric tunnel memristor, Nano Lett. **12**, 5697 (2012).

[5] X. Wang, C. Zhu, Y. Deng, and R. Duan, Author correction: Van der Waals engineering of ferroelectric heterostructures for long-retention memory, Nat. Commun. **12**, 2821 (2021).

[6] R. Guo, W. Lin, X. Yan, T. Venkatesan, and J. Chen, Ferroic tunnel junctions and their application in neuromorphic networks, Appl. Phys. Rev. **7**, 011304 (2020).

[7] E. Y. Tsymbal and H. Kohlstedt, Tunneling across a ferroelectric, Science **313**, 181 (2006).

[8] M. Y. Zhuravlev, R. F. Sabirianov, S. S. Jaswal, and E. Y. Tsymbal, Giant Electroresistance in Ferroelectric Tunnel Junctions, Phys. Rev. Lett. **94**, 246802 (2005).

[9] V. S. Borisov, S. Ostanin, S. Achilles, J. Henk, and I. Mertig, Spin-dependent transport in a multiferroic tunnel junction: Theory for Co/$PbTiO_3$/Co, Phys. Rev. B **92**, 075137 (2015).

[10] L. L. Tao and J. Wang, Ferroelectricity and tunneling electroresistance effect driven by asymmetric polar interfaces in all-oxide ferroelectric tunnel junctions, Appl. Phys. Lett. **108**, 062903 (2016).

[11] K. Klyukin, L. L. Tao, E. Y. Tsymbal, and V. Alexandrov, Defect-Assisted Tunneling Electroresistance in Ferroelectric Tunnel Junctions, Phys. Rev. Lett. **121**, 056601 (2018).

[12] N. A. Benedek and C. J. Fennie, Why are there so few perovskite ferroelectrics? J. Phys. Chem. C **117**, 13339 (2013).

[13] B. Meyer and D. Vanderbilt, *Ab initio* study of $BaTiO_3$ and $PbTiO_3$ surfaces in external electric fields, Phys. Rev. B **63**, 205426 (2001).

[14] D. D. Fong, G. B. Stephenson, S. K. Streiffer, J. A. Eastman, O. Auciello, P. H. Fuoss, and C. Thompson, Ferroelectricity in ultrathin perovskite films, Science **304**, 1650 (2004).

[15] C. Cui and F. Xue, Two-dimensional materials with piezoelectric and ferroelectric functionalities, npj 2D Materials and Applications **2**, 18 (2018).

[16] V. Garcia and M. Bibes, Ferroelectric tunnel junctions for information storage and processing, Nat. Commun. **5**, 4289 (2014).

[17] K. Chang, J. Liu, H. Lin, N. Wang, K. Zhao, A. Zhang, F. Jin, Y. Zhong, X. Hu, W. Duan, Q. Zhang, L. Fu, Q.-K. Xue, X. Chen, and S.-H. Ji, Discovery of robust in-plane ferroelectricity in atomic-thick SnTe, Science **353**, 274 (2016).

[18] K. Chang, T. P. Kaloni, H. Lin, A. Bedoya-Pinto, A. K. Pandeya, I. Kostanovskiy, K. Zhao, Y. Zhong, X. Hu, Q.-K. Xue, X. Chen, S.-H. Ji, S. Barraza-Lopez, and S. S. P. Parkin, Enhanced spontaneous polarization in ultrathin SnTe films with layered antipolar structure, Adv. Mater. **31**, 1804428 (2019).

[19] C. Liu, W. Wan, J. Ma, W. Guo, and Y. Yao, Robust ferroelectricity in two-dimensional SbN and BiP, Nanoscale **10**, 7984 (2018).

[20] W. Wan, C. Liu, W. Xiao, and Y. Yao, Promising ferroelectricity in 2D group IV tellurides: A first-principles study, Appl. Phys. Lett. **111**, 132904 (2017).

[21] C. Cui, W. Hu, X. Yan, C. Addiego, W. Gao, Y. Wang, Z. Wang, L. Li, Y. Cheng, P. Li, X. Zhang, H. N. Alshareef, T. Wu, W. Zhu, X. Pan, and L.-J. Li, Intercorrelated in-plane and out-of-plane ferroelectricity in ultrathin two-dimensional layered semiconductor In_2Se_3, Nano Lett. **18**, 1253 (2018).

[22] J. Xiao, H. Zhu, Y. Wang, W. Feng, Y. Hu, A. Dasgupta, Y. Han, Y. Wang, D. A. Muller, L. W. Martin, P. A. Hu, and X. Zhang, Intrinsic Two-Dimensional Ferroelectricity with Dipole Locking, Phys. Rev. Lett. **120**, 227601 (2018).

[23] W. Ding, J. Zhu, and W. Zhu, Prediction of intrinsic two-dimensional ferroelectrics in In_2Se_3 and other III_2-VI_3 van der Waals materials, Nat. Commun. **8**, 14956 (2017).

[24] A. Belianinov, Q. He, A. Dziaugys, P. Maksymovych, E. Eliseev, A. Borisevich, A. Morozovska, J. Banys, Y. Vysochanskii, and S. V. Kalinin, $CuInP_2S_6$ room temperature layered ferroelectric, Nano Lett. **15**, 3808 (2015).

[25] F. Liu and L. You, Room-temperature ferroelectricity in $CuInP_2S_6$ ultrathin flakes, Nat. Commun. **7**, 12357 (2016).

[26] A. Chandrasekaran, A. Mishra, and A. K. Singh, Ferroelectricity, antiferroelectricity, and ultrathin 2D electron/hole gas in multifunctional monolayer MXene, Nano Lett. **17**, 3290 (2017).

[27] B. Xu, H. Xiang, Y. Xia, K. Jiang, X. Wan, J. He, J. Yin, and Z. Liu, Monolayer $AgBiP_2Se_6$: An atomically thin ferroelectric semiconductor with out-plane polarization, Nanoscale **9**, 8427 (2017).

[28] L. Kang, P. Jiang, H. Hao, Y. Zhou, X. Zheng, L. Zhang, and Z. Zeng, Giant tunneling electroresistance in two-dimensional ferroelectric tunnel junctions with out-of-plane ferroelectric polarization, Phys. Rev. B **101**, 014105 (2020).

[29] L. Kang, P. Jiang, H. Hao, Y. Zhou, X. Zheng, L. Zhang, and Z. Zeng, Giant tunnel electroresistance in ferroelectric tunnel junctions with metal contacts to two-dimensional ferroelectric materials, Phys. Rev. B **103**, 125414 (2021).

[30] H. Bai, X. Li, H. Pan, P. He, Z. Xu, and Y. Lu, Van der Waals antiferroelectric magnetic tunnel junction: A first-principles study of a $CrSe_2/CuInP_2S_6/CrSe_2$ Junction, ACS Appl. Mater. Interfaces **13**, 60200 (2021).

[31] X. Shen, Y. Fang, B. Tian, and C. Duan, Two-dimensional ferroelectric tunnel junction: The case of monolayer In:SnSe/SnSe/Sb:SnSe homostructure, ACS Applied Electronic Materials **1**, 1133 (2019).

[32] J. Ding, D.-F. Shao, M. Li, L.-W. Wen, and E. Y. Tsymbal, Two-Dimensional Antiferroelectric Tunnel Junction, Phys. Rev. Lett. **126**, 057601 (2021).

[33] G. Kresse and J. Furthmüller, Efficient iterative schemes for *ab initio* total-energy calculations using a plane-wave basis set, Phys. Rev. B **54**, 11169 (1996).

[34] G. Kresse and D. Joubert, From ultrasoft pseudopotentials to the projector augmented-wave method, Phys. Rev. B **59**, 1758 (1999).

[35] P. E. Blöchl, Projector augmented-wave method, Phys. Rev. B **50**, 17953 (1994).

[36] J. P. Perdew, K. Burke, and M. Ernzerhof, Generalized Gradient Approximation Made Simple, Phys. Rev. Lett. **77**, 3865 (1996).

[37] L. Bengtsson, Dipole correction for surface supercell calculations, Phys. Rev. B **59**, 12301 (1999).

[38] J. Maassen, M. Harb, V. Michaud-Rioux, Y. Zhu, and H. Guo, Quantum transport modeling from first principles, Proc. IEEE **101**, 518 (2013).

[39] J. Taylor, H. Guo, and J. Wang, *Ab initio* modeling of quantum transport properties of molecular electronic devices, Phys. Rev. B **63**, 245407 (2001).

[40] X. Li, X. Zuo, H. Li, L. Han, Q. Gao, D. Li, B. Cui, D. Liu, and F. Qu, Exotic magnetism in As-doped α/β-In_2Se_3 monolayers with tunable anisotropic carrier mobility, Phys. Chem. Chem. Phys. **21**, 19234 (2019).

[41] L. Kang, P. Jiang, N. Cao, H. Hao, X. Zheng, L. Zhang, and Z. Zeng, Realizing giant tunneling electroresistance in two-dimensional graphene/BiP ferroelectric tunnel junction, Nanoscale **11**, 16837 (2019).

[42] M. Zhao, G. Gou, X. Ding, and J. Sun, An ultrathin two-dimensional vertical ferroelectric tunneling junction based on $CuInP_2S_6$ monolayer, Nanoscale **12**, 12522 (2020).

[43] C. Chan, K. Ho, and K. Bohnen, in *Physical Structure, Handbook of Surface Science*, edited by W. Unertl (North-Holland, 1996), Vol. 1, pp. 101–136.

[44] A. V. Krukau, O. A. Vydrov, A. F. Izmaylov, and G. E. Scuseriaa, Influence of the exchange screening parameter on the performance of screened hybrid functionals, J. Chem. Phys. **125**, 224106 (2006).